ELECTROCHEMISTRY

Accelerating water dissociation in bipolar membranes and for electrocatalysis

Sebastian Z. Oener*, Marc J. Foster, Shannon W. Boettcher*

Catalyzing water dissociation (WD) into protons and hydroxide ions is important both for fabricating bipolar membranes (BPMs) that can couple different pH environments into a single electrochemical device and for accelerating electrocatalytic reactions that consume protons in neutral to alkaline media. We designed a BPM electrolyzer to quantitatively measure WD kinetics and show that, for metal nanoparticles, WD activity correlates with alkaline hydrogen evolution reaction activity. By combining metal-oxide WD catalysts that are efficient near the acidic proton-exchange layer with those efficient near the alkaline hydroxide-exchange layer, we demonstrate a BPM driving WD with overpotentials of <10 mV at 20 mA·cm^{-2} and pure water BPM electrolyzers that operate with an alkaline anode and acidic cathode at 500 mA·cm^{-2} with a total electrolysis voltage of ~2.2 V.

Bipolar membranes (BPMs) consist of a polymeric cation-exchange layer (CEL) with fixed anionic groups and mobile cations in contact with an anion-exchange layer (AEL) with fixed cationic groups and mobile anions (*1*). When a sufficient bias is applied across a BPM, heterolytic water dissociation (WD), $H_2O \rightarrow H^+ + OH^-$, occurs at the AEL/CEL interface, with the H^+ driven through the CEL and the OH^- driven through the AEL (Fig. 1) (*2*). BPMs are used in electrodialysis, desalination, acid-base synthesis, or other electrochemical applications in which a steady-state difference in pH across the membrane is needed (*3*). Emerging applications include the use of BPMs in water (photo)electrolysis ($2H_2O \rightarrow 2H_2 + O_2$), in which the anode and cathode electrocatalyst can operate at a different local pH at steady state (*4*); in CO_2 electrolyzers, in which BPMs attenuate dissolved (bi)carbonate crossover because of the outward flux of H^+/OH^- (*5*–*9*); or in regenerative fuel cells that provide ideal pH conditions for bifunctional electrocatalysts (*10*).

State-of-the-art research and commercial BPMs typically show substantial overpotentials driving water dissociation (η_{wd}) of $\gtrapprox$ 100 mV even at current densities of only ~20 mA·cm^{-2} (table S1; see the supplementary text and figs. S1 and S2 for a precise definition of η_{wd}, including theory and simulation of BPMs). The best-reported BPM uses a three-dimensional (3D) electrospun AEL/CEL junction that passes ~0.5 A·cm^{-2} at η_{wd} ~0.6 V, with $Al(OH)_3$ nanoparticles catalyzing WD at the AEL/CEL interface and neutral salt solutions on both sides of the membranes (*11*). These η_{wd} values are too high for energy-conversion applications that probably require η_{wd} <100 mV at 1 to 2 A·cm^{-2}.

To improve BPM performance, the WD reaction must be accelerated. The addition of polymers such as sulfonated polyether ether ketone (*12*) or metal (hydr)oxide WD catalysts in the BPM junction, e.g., Al_2O_3, $Fe(OH)_3$, and $Cr(OH)_3$, can reduce η_{wd} compared with BPMs without catalyst (*13*–*17*). WD catalysts have also been introduced by the precipitation of metal salts (*17*), by sol-gel chemistry (*14*), or by the addition of nanoparticles (*15*). Previous studies investigated few WD catalysts at a time or focused on the membrane end groups at the AEL/CEL interface (*18*–*22*) and usually treated WD as occurring in a homogeneous, pH-neutral layer. Other polymers are often added in the junction to physically link the constituent layers, and a variety of ionomer membranes (with different chemical end groups and thus different inherent WD kinetics) have been used across different studies. Sometimes, membranes are physically roughened before assembly (*23*). So far, no systematic and comprehensive studies of WD as a function of catalyst composition and location inside the BPM junction have been reported, no consistent mechanistic picture has emerged, and the resulting BPM performance is insufficient for emerging applications (*24*, *25*).

Beyond BPMs, WD is important for any chemical reaction that uses water as a reactant. Understanding fundamental WD mechanisms in pure water, and the reverse H^+/OH^- recombination reaction, has been a focus of experiment and theory for decades (*26*–*28*). The related dissociative adsorption of water, $H_2O \rightarrow H_{ad} + OH_{ad}$, occurs on surfaces and is important when water reacts in thermochemical processes, such as for water-gas-shift catalysis (*29*). The interaction of water with surfaces has thus been of longstanding interest (*30*), with broad importance to corrosion, passivation, and geological processes (*31*). In biology, metalloenzymes activate water. Carbonic anhydrase, for example, binds water to

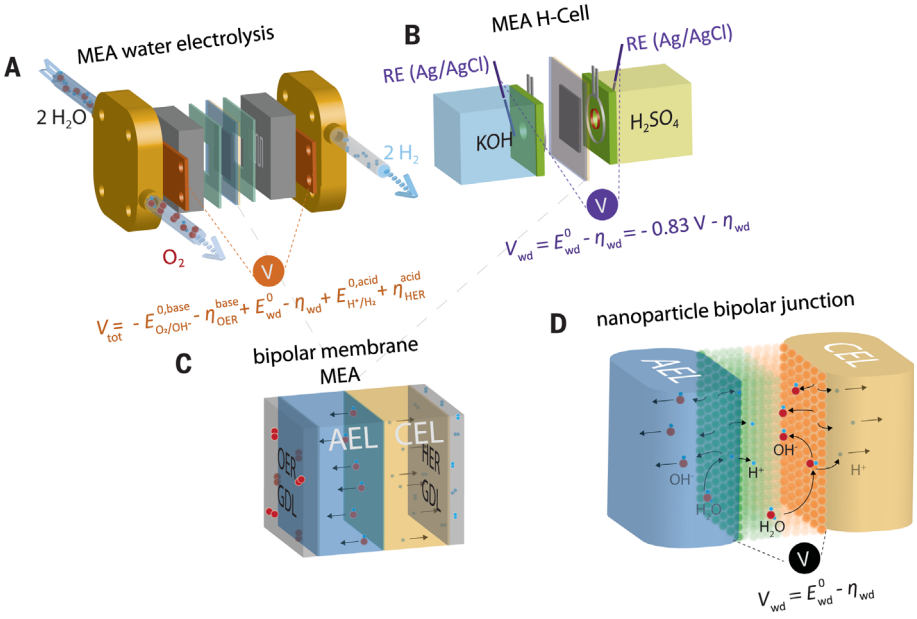

Fig. 1. BPM water-dissociation measurements. (**A**) WD is studied in an electrolyzer fed only pure water. The applied V_{tot} is negative, associated with the positive ΔG_{rxn} of water electrolysis. We define η_{wd} as positive. (**B**) A custom H-cell allows for the direct measurement of η_{wd} to calibrate the electrolysis setup. (**C**) The MEA is kept under constant mechanical pressure, preventing delamination. The MEA is composed of the anode and cathode gas-diffusion layers (GDLs) with IrO_2 OER catalyst and Pt HER catalyst, the AEL and CEL, and the WD catalyst. (**D**) Different nanoparticle WD catalysts can be placed on both the acidic CEL and basic AEL surfaces.

Department of Chemistry and Biochemistry, the Materials Science Institute, and the Oregon Center for Electrochemistry, University of Oregon, Eugene, OR 97403, USA.
*Corresponding author. Email: szo@uoregon.edu (S.Z.O.); swb@uoregon.edu (S.W.B.)

Zn^{2+} and releases H^+ to generate nucleophilic OH^- that reacts with CO_2 to form HCO_3^- (*32*). During the alkaline hydrogen-evolution reaction (HER, $2H_2O + 2e^- \rightarrow H_2 + 2OH^-$), important for low-cost alkaline water electrolysis (*33*), the first step involves WD coupled with the formation of a surface metal hydride ($H_2O + M^* + e^- \rightarrow M\text{-}H + OH^-$) and is thought to be rate limiting. Modification of metals with hydroxides, proposed to catalyze WD, substantially increases HER activity through a possible bifunctional mechanism (*34*, *35*), but alternative explanations have been proposed (*36*–*38*). No direct measurements of the isolated WD step, independent from the other reaction steps, have been conducted on electrocatalysts. WD was also hypothesized to affect the rate of electrocatalytic CO_2 reduction—a reaction that occurs in neutral to basic pH and therefore must use water as a proton source (*39*).

Here, we report the use of a BPM electrolyzer (Fig. 1) to measure WD kinetics on ~40 metal and metal-oxide nanoparticle assemblies composed of ~30 different materials. The electrolyzer was fed only 18.2 MΩ · cm water (without supporting electrolyte that might complicate results; Fig. 1A). The BPMs were encompassed in a membrane-electrode assembly (MEA) held under pressure by two rigid current collectors (Ti/Pt-frit) to prevent delamination and to ensure constant contact between the gas-diffusion electrodes, membranes, and WD-catalyst layers. As different WD catalysts were studied, the materials and preparation parameters used for the MEA were kept constant.

The voltage needed for BPM water electrolysis (V_{tot}) can be conceptually decomposed into the following: (i) the thermodynamic potential of generating O_2 in alkaline media and H_2 in acidic media ($E^{0,acid}_{H^+/H_2} - E^{0,base}_{O_2/OH^-} = -0.40$ V, although, rigorously, the reference half-reactions that define the E^0 on each side of the BPM are at different electrostatic potentials); (ii) the OER and HER overpotentials at a given current density (η_{OER} and η_{HER}, respectively); (iii) the thermodynamic potential needed to generate acid and base from a neutral aqueous solution ($E^0_{wd} = -\Delta G^0_{wd}/F = -0.83$ V at standard conditions); (iv) η_{wd} (defined to be positive here); and (v) the voltage loss caused by ohmic resistance, which is negligible at 20 mA·cm^{-2} for the MEA setup (*40*). We found that V_{tot} depends sensitively on the WD catalyst.

To quantify η_{wd} independently of the anode and cathode reactions, we built an H-cell that maintains the BPM MEA under pressure while contacting the CEL with 1.0 M acid and the AEL with 1.0 M base (Fig. 1B). The electrostatic potential across the BPM was measured using two pH-independent Ag/AgCl reference electrodes in the basic and acidic compartments while a constant current was passed between the anode and cathode (*2*). The η_{wd} values are taken as the increase in the magnitude of the electrostatic potential over the expected equilibrium value as a function of the current density (see the supplementary materials). Because we used high-conductivity electrolytes, and the anode and cathode were in direct contact with the BPM, resistive voltage losses between the BPM and reference electrodes were negligible (fig. S3). By measuring a BPM made with the same IrO_2 WD catalyst in both the H-cell and pure water electrolyzer, we calculated a theoretical electrolyzer baseline for $\eta_{wd} = 0$ V (figs. S4 to S7). Voltages measured for the BPM electrolyzer above this baseline are taken as η_{wd}.

The use of an electrolyzer to study WD kinetics inside the BPM instead of a conventional H-cell is important. We fed pure water, thereby eliminating co-ion (e.g., K^+, Cl^-) crossover in the conventional H-cell measurements that could carry current and potentially influence the WD reaction at the AEL/CEL junction through ion adsorption (*36*, *41*, *42*). In the pure water BPM electrolyzer, current is only carried by H^+ and OH^-. We used IrO_2 WD catalysts to calibrate the electrolyzer with the H-cell measurements because IrO_2 is stable under acidic and alkaline conditions. Co-ions in the H-cell setup are responsible for <2% of the current at 20 mA·cm^{-2} (fig. S35).

The calibrated BPM electrolyzer was used to study WD kinetics on metal-oxide nanoparticles deposited in the BPM junction (table S2). We found that η_{wd} is relatively insensitive to loading once the membrane is covered with ~100 to 200 nm of WD catalyst (see figs. S8 and S9). Because metal-oxide surfaces are polyacids and/or polybases, their surface chemistry and protonation state depend on pH, which could affect WD kinetics (*43*, *44*). The CEL surface is an acidic environment, whereas the AEL surface is alkaline. To study the WD catalysis under a defined local pH, we used a chemically stable WD catalyst at one surface (e.g., NiO at the AEL and Sb:SnO_2 at the CEL) while systematically varying the WD catalyst at the other membrane surface (polarization curves are shown in figs. S10 to S15). We separately measured each oxide's point of zero charge (PZC; fig. S16 and table S2) to assess acid-base properties; WD catalyst activity versus PZC is plotted in Fig. 2. With Sb:SnO_2 on the acidic CEL, the best WD catalysts on the basic AEL tend to be those with basic PZCs, such as NiO. With NiO on the basic AEL, the best WD catalysts on the acidic CEL are those with acidic PZCs, such as IrO_2 or SnO_2. At higher current densities, and thus larger η_{wd}, these weak correlations appear more pronounced (fig. S17).

A proton-transfer mechanism, similar to the one proposed for WD catalysis by ionomer-membrane end groups at the AEL/CEL interface (*18*, *19*, *22*), can be used to tentatively rationalize the data in Fig. 2. Under basic conditions at the AEL, most oxide surfaces are negatively charged and consist of structurally diverse –OH and –O^- species. These sites might act as proton donors or acceptors,

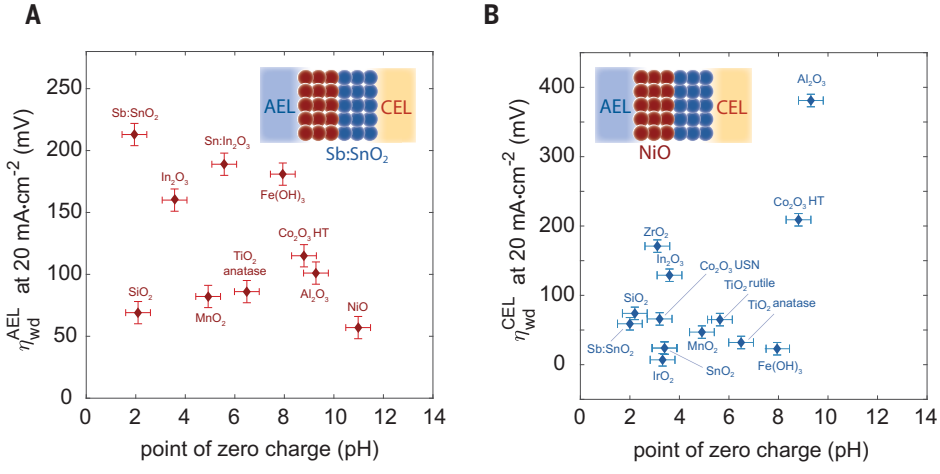

Fig. 2. WD overpotentials and PZC for oxide nanoparticles. (**A**) Values for η_{wd} measured with catalysts placed under locally alkaline conditions in the BPM (η^{AEL}_{wd})using acid-stable Sb:SnO_2 to cover the acidic CEL. (**B**) Values for η_{wd} measured with catalysts placed under locally acidic conditions (η^{CEL}_{wd}) using base-stable NiO to coat the alkaline AEL. The PZCs were measured by finding the pH where the zeta potential (at the hydrodynamic shear plane) tended to zero. The uncertainties in the PZC data are based on measurements made in triplicate (see the supplementary materials and fig. S16), whereas those for η_{wd} reflect the uncertainty of the calibration of the MEA with the H-cell setup (see the supplementary materials and figs. S4 to S6).

respectively, catalyzing WD through a two-step mechanism as follows:

$$MO^- + H_2O \underset{k_1'}{\overset{k_1}{\rightleftarrows}} MOH + OH^- \quad (1)$$

$$MOH + H_2O \underset{k_2'}{\overset{k_2}{\rightleftarrows}} MO^- + H_3O^+ \quad (2)$$

In the above case, MO^- would be a catalyst active site, with MOH an intermediate. Under acidic conditions at the CEL, most oxide surfaces will be protonated, consisting of -OH_2^+ and -OH species, and can similarly catalyze WD as follows:

$$MOH_2^+ + H_2O \underset{k_3'}{\overset{k_3}{\rightleftarrows}} MOH + H_3O^+ (3)$$

$$MOH + H_2O \underset{k_4'}{\overset{k_4}{\rightleftarrows}} MOH_2^+ + OH^- (4)$$

A large net rate for either of the above two-step mechanisms requires sufficient concentrations of both the protonated and unprotonated surface species (assuming similarity of the forward rate constants k_1 and k_2 or k_3 and k_4), so that both steps are simultaneously fast. At local pH values near the PZC, a diversity of surface protonation states capable of driving both steps is needed for fast WD. Although this is consistent with the observation that oxide WD catalysts tend to work best when the local pH is near the PZC, the weak trends shown in Fig. 2 illustrate that other factors, such as accessible surface area, the diversity and range of surface pK_a, and the density of surface hydroxyl groups, are also likely to affect WD activity. For materials without a substantial density of ionizable surface groups (e.g., noble metals) PZC data are unlikely to be useful.

Although alternative mechanisms involving the dissociative adsorption of water to form M–OH intermediates are also possible (see the supplementary materials), we hypothesize that these pathways are slow on typical oxides because of the strength of the M–O bonds. Such mechanisms may be prevalent on the precious metals discussed below. A few oxides, e.g., TiO_2 and SiO_2, catalyze WD reasonably in both acidic and basic environments. This may be because of the broad surface pK_a range for TiO_2 and SiO_2 (*45*, *46*), which are better described as "spectra" than discrete pK_a values (*44*). Some oxides are also not stable in acid or base. NiO, for example, would partially dissolve on the CEL surface generating soluble Ni^{2+} that can ion exchange for H^+ in the CEL. Improved mechanistic insight will require a better understanding of the WD-catalyst surface speciation. Raman and Stark effect spectroscopy, for example, might be suitable to detect chemical changes on the catalyst surface during operation and help to elucidate the role of the electric field in the junction, respectively.

These findings suggest a new principle for the design of WD catalysts that accounts for the surface speciation and chemical stability

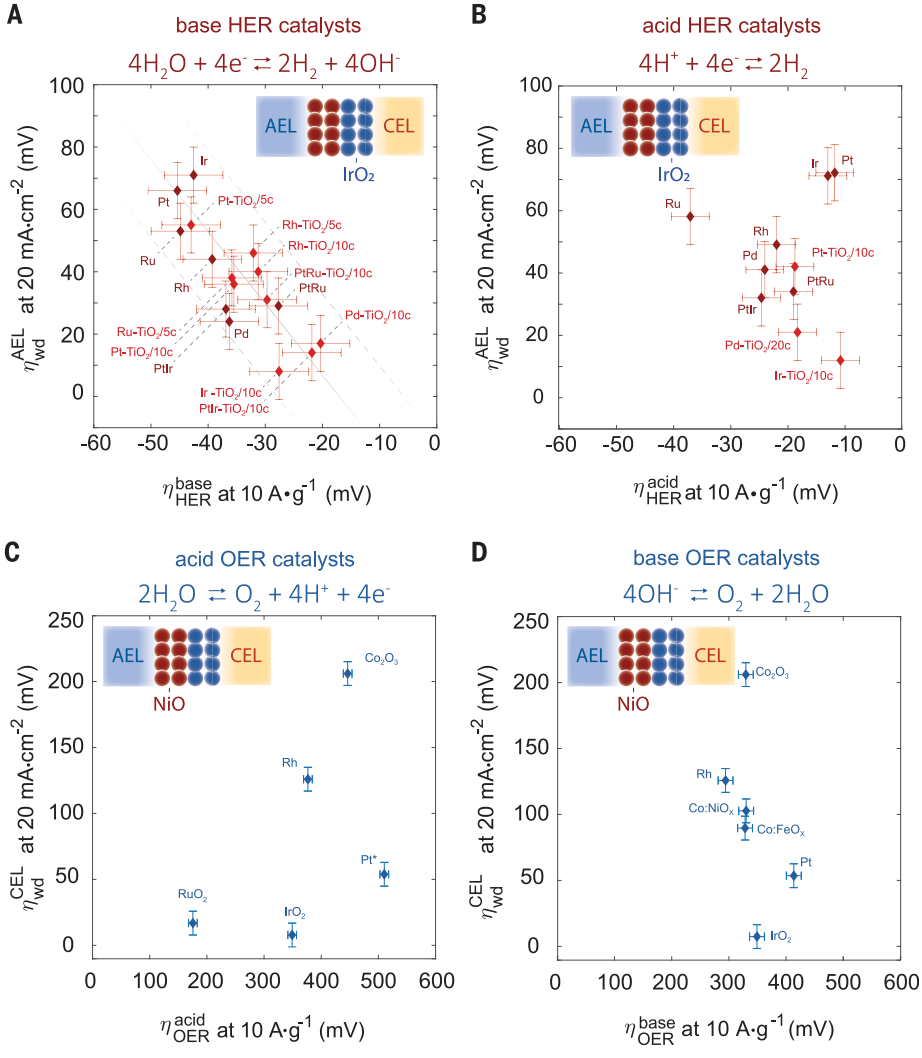

Fig. 3. Comparison between WD and electrocatalytic overpotentials measured on the same nanoparticles. (**A**) The overpotentials for WD in a locally basic environment (with IrO_2 used as the stable WD catalyst on the acidic CEL surface) correlate with the overpotentials measured for HER in 1.0 M KOH [$\rho(\eta_{HER}^{base}, \eta_{wd}^{AEL})$ = −0.81], consistent with WD rate limiting the alkaline HER. (**B**) No correlation is found between η_{wd} and the HER performance in 1.0 M H_2SO_4 [$\rho(\eta_{HER}^{acid}, \eta_{wd}^{AEL})$ = −0.13], consistent with WD not being involved in the acidic HER mechanism. Dark-red markers in (A) and (B) show the as-received nanoparticles and light-red markers show the samples after TiO_2 decoration. (**C**) The η_{wd} in a locally acidic environment (with NiO used as the stable WD catalyst on the basic AEL surface) do not strongly correlate with the overpotentials measured for OER in 1.0 M H_2SO_4 [$\rho(\eta_{OER}^{acid}, \eta_{wd}^{CEL})$ = 0.49], consistent with WD not being rate limiting. (**D**) No strong correlation is present between η_{wd} and the OER overpotentials in 1.0 M KOH [$\rho(\eta_{OER}^{base}, \eta_{wd}^{CEL})$ = −0.45], consistent with the large OH^- concentration obviating the need for WD. The loadings for the electrocatalysis studies were 0.1 to 1 mg · cm^{-2} and the current densities were 1 to 10 mA·cm^{-2}, similar to the WD current densities studied in the BPM. The currents for the electrocatalysts are normalized to mass because higher loadings lead to larger current. The WD current was not normalized to mass because a simple correlation between activity and loading does not exist (see fig. S8). The uncertainties for the OER and HER overpotentials are based on the average standard deviation obtained for each electrolyte condition, whereas those for η_{wd} reflect the uncertainty of the MEA calibration with the H-cell setup (see the supplementary materials and figs. S4 to S6). The Pt OER activity degraded with subsequent cycles because of oxidation (see the supplementary materials).

of the catalyst at the relevant local pH. In the context of BPMs, the data show the superiority of using two WD catalyst layers selected for the appropriate local pH over a single material as in prior work. We envision designing multilayered WD catalysts that provide a gradient in surface acid-base behavior matched to the pH gradient present at the AEL/CEL interface at the operational current density.

The new data also suggest that catalysis of WD is more important than electric-field enhancement (Onsager's theory of the second Wien effect) in the BPM junction, a topic of a long-standing debate (*18*, *24*, *47*, *48*). The electric field across the AEL/CEL junction is ~ $3 \cdot 10^4$ V · cm^{-1}, assuming the electrostatic potential drops linearly across an ~300-nm-thick WD-catalyst layer. This field is not sufficient to substantially increase the rate of WD based on Onsager's theory (see the supplementary materials) (*47*), consistent with previous calculations (*49*). We observed no apparent correlation between η_{wd} and the electronic properties of the oxide. Electrical conductors (IrO_2, RuO_2), *n*- and *p*-type semiconductors (SnO_2, NiO), and insulators (SiO_2) all modify and/or screen the electric field distribution inside the WD-catalyst layer differently yet are all efficient WD catalysts. The η_{wd} values are also temperature dependent (fig. S18). The BPM made without added WD catalyst has the narrowest junction, sharpest electrochemical potential gradient, and thus the largest electric field, but the performance is the worst (see below). These findings suggest the rates of WD are influenced primarily by surface catalysis in the presence of gradients in $\bar{\mu}_{H^+}$ and $\bar{\mu}_{OH^-}$ that separate H^+ from OH^-, with electric field enhancement playing a secondary role.

WD has further been proposed to be rate determining in some electrocatalytic reactions. During the HER in alkaline media ($2H_2O + 2e^- \rightarrow H_2 + 2OH^-$), the first step ($H_2O + e^- \rightarrow H_{ad} + OH^-$) involves WD and metal hydride formation and is thought to be the reason HER is slower in base than in acid (*34*, *35*). The OER under acidic or neutral conditions, $2H_2O \rightarrow O_2 + 4H^+ + 4e^-$, likewise requires WD to generate -OH_{ad} species that can be further oxidized. WD, however, is not thought to be rate limiting for the OER (*50*). A fundamental challenge is the inability to isolate and measure WD kinetics for a particular electrocatalyst independent of other electrochemical processes. Traditionally, the driving force for both WD and electron transfer is simultaneously provided as an applied electrode potential. Here, we isolate WD kinetics by locally generating a gradient in the electrochemical potentials $\bar{\mu}_{H^+}$ and $\bar{\mu}_{OH^-}$ inside the electrically disconnected BPM junction (see the supplementary materials for simulations).

We used the BPM electrolyzer to measure η_{wd} of common HER and OER electrocatalysts (Fig. 3) and analyzed them to ascertain whether η_{wd} correlates with electrocatalytic overpotentials (at similar current density) measured for the same particles in a three-electrode cell (figs. S19 to S23). We found that η_{HER} of precious metal nanoparticles in 1.0 M KOH linearly correlates with η_{wd} measured at the basic AEL surface (Pearson correlation coefficient $\rho(\eta_{HER}^{base}, \eta_{wd}^{AEL}) = -0.81$). As η_{wd} tends to zero, so does η_{HER} at a similar current density. When η_{HER} for those metal nanoparticles is measured in 1.0 M H_2SO_4, where WD is not needed for the HER, there is no significant correlation and $\rho(\eta_{HER}^{acid}, \eta_{wd}^{AEL}) = -0.13$.

The above correlation is consistent with the hypothesis that modifying metals such as Pt with metal hydroxides such as $Ni(OH)_2$ improves alkaline HER activity because of increased WD kinetics (*34*, *35*). Our results show that NiO (which is hydroxylated in water) is an excellent alkaline WD catalyst and will further enable the design of new electrocatalysts. TiO_2 is an active WD catalyst in both acid and base and is chemically stable. We deposited TiO_2 by atomic-layer deposition (ALD) onto Pt, Ir, Ru, Rh, PtRu, and PtIr nanoparticles at 250°C. The addition of TiO_2 simultaneously decreased both η_{wd} and η_{HER}^{base}, providing direct support to a bifunctional alkaline HER mechanism in which the oxide facilitates WD and the metal stabilizes M–H intermediates.

A water-ordering model has been alternatively proposed to explain the increased alkaline HER kinetics of metal-hydroxide-functionalized Pt (*37*). When water is dissociated during HER in base, OH^- is produced and stabilized (i.e. solvated) by orienting nearby water dipoles. Pt, under alkaline HER conditions, carries a substantial surface charge, which also orients nearby water molecules and generates an energy barrier to water reorganization. $Ni(OH)_2$ lowers the surface charge of Pt under alkaline HER conditions, which could reduce the water reorganization energy and thus η_{HER}^{base} (*37*). Although the general trends of PZC with WD rate (Fig. 2) are consistent with this hypothesis, some of our data are not. SiO_2 has an acidic PZC yet works well for WD in base, where it presents charged surfaces that would, in the above model, be expected to retard WD. TiO_2 and $Ni(OH)_2$ have very different PZCs, and thus are expected to have very different net surface charge densities in base. However, both enhance alkaline HER kinetics on Pt and other metal surfaces. This evidence, along with the proposed proton-transfer WD mechanism (Eqs. 1 to 4), favors a bifunctional route for alkaline HER on (hydr)oxide-functionalized metal surfaces. Further work is needed, however, to understand the effects of water ordering on WD activity for the oxides studied here, which are likely to have a diversity of hydroxylated surface sites with a range of pK_a values.

In contrast to alkaline HER, we did not find a strong correlation between η_{wd} and the OER activity in acid [$\rho(\eta_{OER}^{acid}, \eta_{wd}^{CEL}) = 0.49$], where H_2O is also a reagent (Fig. 3C), nor between η_{wd} and the OER activity in base [$\rho(\eta_{OER}^{base}, \eta_{wd}^{CEL}) = -0.45$]. This is consistent with computational models of OER indicating that nonoptimal M–O binding strengths provide rate-limiting barriers (*50*). It is, however, interesting that fast acid-OER catalysts, such as RuO_2 and IrO_2, are also fast WD catalysts.

Although the durability of the WD catalysts in the BPM have not been studied extensively, the observed trends (Figs. 2 and 3) cannot be explained by differences in WD catalyst stability or dissolution (which might provide current-carrying ions or be coupled to WD). The electrolyzer measurements used pure water without soluble electrolyte, and therefore crossover of acid or base into the BPM junction is avoided. The best WD catalysts (IrO_2 in acid and NiO in base) should not substantially

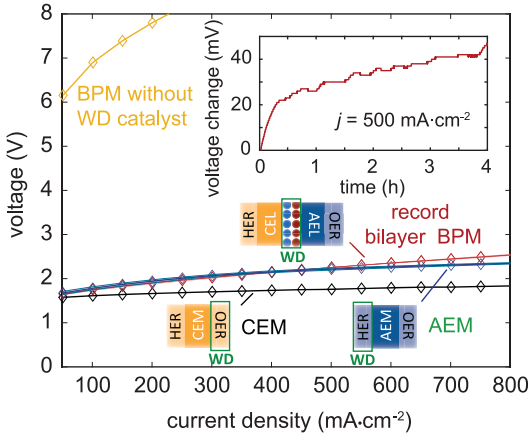

Fig. 4. Alkaline, acidic, and BPM electrolyzers. BPM electrolyzers require >6 V to drive electrolysis at 50 mA·cm^{-2} without additional WD catalysts (yellow). When the new bilayer WD catalysts are added, the performance substantially improves and is similar to a reference AEM electrolyzer. The PEM electrolyzer performs better, which is likely because of the superior properties of Nafion compared with Sustainion. For all electrolyzers, the cathode and anode catalyst composition and loading were identical. The AEM and bilayer BPM electrolyzer polarization curves are averages over three devices and/or datasets, with the error indicated by the thickness of the line (fig. S32). The inset shows that the BPM electrolyzer performance is relatively stable over 4 hours of operation at 500 mA·cm^{-2} (see the supplementary materials for discussion of degradation modes and mitigation strategies).

dissolve based on thermodynamic data (*51*). The rate of voltage increase for the BPM electrolyzer is also not correlated with η_{wd} (figs. S24 to S30), and continuous operation for >4 hours at 500 mA·cm^{-2} leads to an increase of only 40 mV in the BPM electrolysis voltage (Fig. 4).

Taken together, these results help to unify concepts of WD catalysis across the membrane and electrocatalysis sciences. The BPM electrolyzer architecture allows WD reaction rates to be directly probed in relevant acidic or basic local-pH environments and independently of electron-transfer processes. Bifunctional HER catalysts, as demonstrated by others (*34*, *35*) and shown here for Pt/TiO_2, can now be assembled based on independently measured WD activity. This approach should facilitate the design of electrocatalysts for any electrochemical process that uses water as a reactant (including the electrochemical reduction of CO_2 and N_2).

The BPMs fabricated here also have faster WD kinetics than those previously reported (see table S1 for η_{wd} values). The best BPMs, e.g., those with NiO or IrO_2 coated with 10 layers of TiO_2 by ALD (Ir/TiO_2-10c) at the AEL surface and RuO_2 or IrO_2 at the CEL surface, show η_{wd} that is within measurement error (±9 mV) of 0 mV at 20 mA·cm^{-2} in pure water at 50°C. Fig. S31 shows a comparison of a NiO|IrO_2 bilayer BPM with other BPMs measured under comparable H-cell conditions at 25°C. Commercial membranes, e.g., those from Fumatech, show η_{wd} ranging from 100 to 200 mV at 20 mA·cm^{-2} (depending on pretreatment). Research BPMs generally show similar or substantially higher η_{wd} [see fig. S31, table S1, and (*52*)]. Figure 4 compares the polarization curves of our best BPM pure water electrolyzers to reference alkaline-exchange membrane (AEM) and proton-exchange membrane (PEM) electrolyzers, which are made from the same membranes and OER/HER electrocatalysts. The BPM electrolyzers meet or exceed the performance of the AEM electrolyzers up to 400 mA·cm^{-2}. This is possible because, in the AEM electrolyzer, Pt must drive HER in alkaline media with relatively slow kinetics. In the BPM electrolyzer, Pt drives HER with fast kinetics in a locally acidic environment, whereas protons are provided through catalyzed WD in the AEL/CEL junction. This result proves that η_{wd} is relatively small, even at high current densities, for the new BPMs reported here. State-of-the-art 3D junction BPMs, similarly measured with acid and base on each side of the BPM, show η_{wd} of ~1 V at 0.2 A cm^{-2} (*24*). Here, we drove water electrolysis at 0.2 A cm^{-2} with a total voltage of ~1.9 V and an estimated η_{wd} of <0.25 V. For current densities beyond 400 mA·cm^{-2}, the BPM electrolyzer voltage is higher than that of the AEM electrolyzer. We ascribe this difference to water-transport limitations and ionic series resistance inside the BPM junction (see the supplementary materials).

Further innovations are possible to improve performance and achieve small η_{wd} at the ~2 A cm^{-2} relevant to many technologies. Examples include engineering the surface area and surface chemistry of the WD catalyst, the number of different WD-catalyst layers, the interfacial area with a 3D junction (*11*, *24*), the ionomer thickness and chemistry to improve water transport to the AEL/CEL junction, and the ionic conductivity in the WD catalyst layer. The performance decay (Fig. 4, inset), which may be related to junction dehydration at high currents, must also be mitigated before commercial application (see the supplementary materials).

The BPM enables electrochemical devices in which ideal pH conditions can be selected independently for each half-reaction, in contrast to traditional architectures, in which electrode stability, catalyst activity, and cost must be simultaneously optimized at both cathode and anode for a single pH. This system design flexibility could enable high-performance, nonprecious metal BPM electrolyzers. Earth-abundant metal oxides can be used to catalyze the WD reaction inside the BPM junction, with optimal earth-abundant OER catalysts (e.g., Ni_xFe_yO) at the basic anode and HER catalysts at the acidic cathode. Flow batteries that use anolyte and catholyte at different pH values (*53*, *54*), (regenerative) fuel cells (*10*), and direct CO_2 electrolyzers that prevent soluble co-ion crossover (*7*) are other emerging applications facilitated by high-performance BPMs.

REFERENCES AND NOTES

1. T. Luo, S. Abdu, M. Wessling, *J. Membr. Sci.* **555**, 429–454 (2018).
2. R. S. Reiter, W. White, S. Ardo, *J. Electrochem. Soc.* **163**, H3132–H3134 (2016).
3. Y. Tanaka, *Ion Exchange Membranes: Fundamentals and Applications* (Elsevier, 2007).
4. D. A. Vermaas, M. Sassenburg, W. A. Smith, *J. Mater. Chem. A Mater. Energy Sustain.* **3**, 19556–19562 (2015).
5. Y. C. Li *et al.*, *ACS Energy Lett.* **1**, 1149–1153 (2016).
6. D. A. Vermaas, W. A. Smith, *ACS Energy Lett.* **1**, 1143–1148 (2016).
7. Y. C. Li *et al.*, *Adv. Sustainable Syst.* **2**, 1700187 (2018).
8. M. Lin, L. Han, M. R. Singh, C. Xiang, *ACS Appl. Energy Mater.* **2**, 5843–5850 (2019).
9. Y. C. Li *et al.*, *ACS Energy Lett.* **4**, 1427–1431 (2019).
10. J. M. Ahlfield, L. Liu, P. A. Kohl, *J. Electrochem. Soc.* **164**, F1165–F1171 (2017).
11. C. H. Shen, R. Wycisk, P. N. Pintauro, *Energy Environ. Sci.* **10**, 1435–1442 (2017).
12. J. Balster *et al.*, *J. Membr. Sci.* **365**, 389–398 (2010).
13. S. S. Mel'nikov, O. V. Shapovalova, N. V. Shel'deshov, V. I. Zabolotskii, *Petrol. Chem.* **51**, 577–584 (2011).
14. A. M. Rajesh, T. Chakrabarty, S. Prakash, V. K. Shahi, *Electrochim. Acta* **66**, 325–331 (2012).
15. F. Hanada, K. Hiraya, N. Ohmura, S. Tanaka, Bipolar membrane and method for its production. European Patent EP0459820B1 (1991).
16. Y. Oda, T. Yawataya, *Desalination* **5**, 129–138 (1968).
17. M.-S. Kang, Y.-J. Choi, H.-J. Lee, S.-H. Moon, *J. Colloid Interface Sci.* **273**, 523–532 (2004).
18. R. Simons, *Nature* **280**, 824–826 (1979).
19. R. Simons, G. Khanarian, *J. Membr. Biol.* **38**, 11–30 (1978).
20. H. Strathmann, H. J. Rapp, B. Bauer, C. M. Bell, *Desalination* **90**, 303–323 (1993).
21. A. B. Yaroslavtsev, V. V. Nikonenko, V. I. Zabolotsky, *Russ. Chem. Rev.* **72**, 393–421 (2003).
22. V. I. Zabolotskii, N. V. Shel'deshov, N. P. Gnusin, *Russ. Chem. Rev.* **57**, 801–808 (1988).
23. A. J. B. Kemperman, *Handbook on Bipolar Membrane Technology* (Twente Univ. Press, 2000).
24. Z. Yan *et al.*, *Energy Environ. Sci.* **11**, 2235–2245 (2018).
25. S. Abdu *et al.*, *ACS Appl. Mater. Interfaces* **5**, 10445–10455 (2013).
26. M. Moqadam *et al.*, *Proc. Natl. Acad. Sci. U.S.A.* **115**, E4569–E4576 (2018).
27. M. Eigen, L. d. Maeyer, *Z. Elecktrochem.* **59**, 986 (1955).
28. G. Ertl, H. Gerischer, *Z. Elecktrochem.* **66**, 560 (1962).
29. C. V. Ovesen, P. Stoltze, J. K. Nørskov, C. T. Campbell, *J. Catal.* **134**, 445–468 (1992).
30. M. Sterrer *et al.*, *J. Mater. Res.* **34**, 360–378 (2019).
31. P. A. Thiel, T. E. Madey, *Surf. Sci. Rep.* **7**, 211–385 (1987).
32. I. Bertini, C. Luchinat, "The reaction pathways of zinc enzymes and related biological catalysts," in *Bioinorganic Chemistry* (University Science Books, 1994), pp. 37–106.
33. D. Xu *et al.*, *ACS Catal.* **9**, 7–15 (2019).
34. N. Danilovic *et al.*, *Angew. Chem. Int. Ed.* **51**, 12495–12498 (2012).
35. R. Subbaraman *et al.*, *Science* **334**, 1256–1260 (2011).
36. X. Chen, I. T. McCrum, K. A. Schwarz, M. J. Janik, M. T. M. Koper, *Angew. Chem. Int. Ed.* **56**, 15025–15029 (2017).
37. I. Ledezma-Yanez *et al.*, *Nat. Energy* **2**, 17031 (2017).
38. J. Zheng, W. Sheng, Z. Zhuang, B. Xu, Y. Yan, *Sci. Adv.* **2**, e1501602 (2016).
39. M. Luo *et al.*, *Nat. Commun.* **10**, 5814 (2019).
40. S. Z. Oener, S. Ardo, S. W. Boettcher, *ACS Energy Lett.* **2**, 2625–2634 (2017).
41. J. N. Mills, I. T. McCrum, M. J. Janik, *Phys. Chem. Chem. Phys.* **16**, 13699–13707 (2014).
42. E. Liu *et al.*, *J. Am. Chem. Soc.* **141**, 3232–3239 (2019).
43. H. P. Boehm, *Discuss. Faraday Soc.* **52**, 264–275 (1971).
44. D. S. Smith, F. G. Ferris, *Environ. Sci. Technol.* **35**, 4637–4642 (2001).
45. X. Liu, J. Cheng, X. Lu, R. Wang, *Phys. Chem. Chem. Phys.* **16**, 26909–26916 (2014).
46. M. K. Ridley, V. A. Hackley, M. L. Machesky, *Langmuir* **22**, 10972–10982 (2006).
47. L. Onsager, *J. Chem. Phys.* **2**, 599–615 (1934).
48. M. A. Blommaert, D. A. Vermaas, B. Izelaar, B. in 't Veen, W. A. Smith, *J. Mater. Chem. A Mater. Energy Sustain.* **7**, 19060–19069 (2019).
49. H. Strathmann, J. J. Krol, H. J. Rapp, G. Eigenberger, *J. Membr. Sci.* **125**, 123–142 (1997).
50. I. C. Man *et al.*, *ChemCatChem* **3**, 1159–1165 (2011).
51. M. Pourbaix, *Atlas of Electrochemical Equilibria in Aqueous Solutions* (National Association of Corrosion, 1974).
52. M. B. McDonald, S. Ardo, N. S. Lewis, M. S. Freund, *ChemSusChem* **7**, 3021–3027 (2014).
53. M. Park *et al.*, *Adv. Energy Mater.* **9**, 1900694 (2019).
54. J. Xia, G. Eigenberger, H. Strathmann, U. Nieken, *J. Membr. Sci.* **565**, 157–168 (2018).
55. S. Z. Oener, M. J. Foster, S. W. Boettcher, Tabulated data for: Accelerating water dissociation in bipolar membranes and for electrocatalysis. Zenodo (2020); .

ACKNOWLEDGMENTS

We thank M. Lonergan for assistance in developing the numerical simulations, S. Ardo for insightful discussions regarding BPM physics and ion-transfer reactions, and J. Fehrs for assistance analyzing ion-crossover rates. **Funding:** This work was supported by the National Science Foundation Chemical Catalysis program under grant no. CHE-1566348. S.Z.O acknowledges support from a research fellowship of the German Research Foundation (Deutsche Forschungsgemeinschaft) under project no. 408246589 (OE 710/1-1). We acknowledge use of shared instrumentation in the CAMCOR and Rapid Materials Prototyping facilities, which are supported by grants from the M. J. Murdock Charitable Trust, the W. M. Keck Foundation, ONAMI, and the NSF. **Author contributions:** S.Z.O and S.W.B. conceived of the project, analyzed the data, and wrote the manuscript. S.Z.O. completed the experiments with assistance from M.J.F. **Competing interests:** S.Z.O, S.W.B., and M.J.F have filed a provisional patent application (U.S. Patent 62/984,652) based on the results of this manuscript. **Data and materials availability:** Tabulated data are available in the Zenodo repository (*55*).

SUPPLEMENTARY MATERIALS

science.sciencemag.org/content/369/6507/1099/suppl/DC1
Materials and Methods
Figs. S1 to S36
Tables S1 and S2
References (*56*–*73*)

15 August 2019; resubmitted 20 December 2019
Accepted 22 June 2020
Published online 2 July 2020
10.1126/science.aaz1487

Accelerating water dissociation in bipolar membranes and for electrocatalysis

Sebastian Z. Oener, Marc J. Foster and Shannon W. Boettcher

Science **369** (6507), 1099-1103.
DOI: 10.1126/science.aaz1487originally published online July 2, 2020

Easing water apart

Traditional setups for splitting water into hydrogen and oxygen operate either in acid or in base. A bipolar membrane can potentially enhance efficiency by bridging acidic hydrogen evolution to basic oxygen evolution. Oener *et al.* undertook a systematic study of how catalysts paired with such a membrane might accelerate the preliminary step of water dissociation into protons and hydroxide ions. Using insights from this study for optimal catalyst integration, they were able to substantially lower the overpotential of a bipolar membrane electrolyzer.

Science, this issue p. 1099